Article:

eprints@whiterose.ac.uk
https://eprints.whiterose.ac.uk/

Contents lists available at ScienceDirect

Tribology International

Friction and wear in railway ballast stone interfaces

B. Suhr [a,*], T.A. Butcher [b], R. Lewis [b], K. Six [a]

[a] *Virtual Vehicle Research GmbH, Graz, Austria*
[b] *Department of Mechanical Engineering, The University of Sheffield, Sheffield, UK*

ARTICLE INFO

ABSTRACT

Particle friction in railway ballast influences strongly the behaviour of ballasted tracks. New challenges posed on railway infrastructure increase the requirement for simulations, which need the friction coefficient as an input parameter. Measured friction coefficients of ballast stone contacts were found only in two studies, both under constant loads. In this work, two types of ballast were investigated in cyclic friction tests with incremental increase of the applied load after several cycles. Before each load increase, 3D-scans of some ballast stones allowed to calculate the contact area. Estimating the stress in the contact, the stress-dependency of the friction coefficient and wear were investigated. These experimental observations are discussed regarding their impact for friction modelling in the simulation of railway ballast.

1. Introduction

In railways, ballasted tracks are the most common form of track systems. One of the main tasks of the ballast is to transfer forces (both in the vertical and lateral directions) from the wheel–rail contact to the ground. How these forces spread within the ballast for different types of operational conditions (e.g. speeds and axle loads, tangent vs. curved track) is still not fully understood.

The Discrete Element Method (DEM), introduced in [1], is a widely used tool for the simulation of railway ballast and/or ballasted tracks, as it takes into account directly the granular nature of the material and thus provides insight into different phenomena occurring at the particle scale. The DEM simulation method also allows the effect of new track components being introduced to be predicted, e.g. different sleepers types, [2]; under sleeper pads, [3,4]; under ballast mats, [4,5]; or geogrids, [5–8]. The settlement behaviour of railway ballast is of high practical importance, but also challenging to model in DEM as several effects can contribute: frictional behaviour and breakage of stones or wear. Compare [4,9–12] for DEM modelling of the mentioned aspects.

For the simulation of railway ballast, many studies in the literature address particle shape modelling: [6,13–16]. The developed accurate particle shape models are computationally demanding and are usually combined with very simple models for particle contact, e.g. the linear spring and dashpot model, [1]. Only a few works exist, aimed at improving contact modelling by taking into account additional physical effects. For example in [17–19], the contact model is modified to include particle edge breakage and yielding.

No matter what contact model is used, the identification of the corresponding parameters is challenging. Coetzee describes two possible approaches in [20]. First, the so-called *bulk calibration approach*, where parameters values are adapted iteratively such that the simulated and measured bulk behaviour of the studied material are in good accordance. Problems with this approach are that several sets of parameters can yield similar or the same simulation results, see [21], and that the physical meaning of the parameters can be lost. Second, in the *direct measurement approach*, the parameters used for the contact models are determined by measuring the corresponding material properties (e.g. Young's modulus) and the coefficient of friction. Such measurements are not always possible or available. Moreover, this strategy can only give correct results if particle size and shape are modelled accurately and if the contact model used reflects all relevant physical effects. As a consequence, a mixture of both approaches is often used. Although the accurate shape modelling of railway ballast is still a topic of active research, the measurement of ballast–ballast friction is one step towards the usage of the direct measurement approach for DEM modelling.

For granular materials, contact friction is a key influencing factor for the shearing behaviour. In DEM simulations, friction is usually modelled with Coulomb's law assuming a constant interparticle friction coefficient. Only a few studies exist where known tribological effects, such as stress-dependency of the friction coefficient, are used in DEM simulations, see [17,22,23]. For railway ballast, the friction coefficient has a big influence on the shear strength of the track. In the cited works

---

which simulate railway ballast [3–19], the friction coefficients used range between 0.4 and 0.8. Two reasons for this relatively wide range are: first, the use of the described parameter variation approach, where the physical meaning of parameters is weakened. Second, only two works in the literature report measured friction coefficients of railway ballast stones which could be used in DEM simulations.

In [24], Kwan presented friction tests on natural ballast stones which were set in epoxy and sheared in a direct shear tester. For five different vertical loads ranging between 65 N and 225 N, two tests per load were shown. The results were summarised in an average friction coefficient of 0.6, although measured results scattered strongly over the reported shear distance of 2.3 mm. This was explained by the unevenness of the stones and the small number of tests. As the contact area in this testing method is unknown, the contact stress cannot be estimated. Therefore, it is unclear if the applied forces correspond to stresses usually occurring in laboratory tests on railway ballast.

In [25], 14 cyclic friction tests on railway ballast were conducted. Relatively sharp ballast tips were sheared over relatively flat ballast areas and the number of applied loading cycles ranged between 100 and 400. In all tests, a vertical load of 1 kN was applied and the total relative displacement was 2.4 mm. Both new ballast grains and previously eroded grains were investigated. Moreover, in half of the tests compressed air was used to remove fines created during shearing. In four tests water was applied to investigate the effect of humid or wet contact conditions. For the calculation of the coefficient of friction a geometry correction was developed to take into account the unevenness of the ballast. Neither the state of the ballast grains (new or eroded) nor the use of compressed air or water had a strong influence on the resulting friction coefficient. The total range of measured friction values was 0.7 to 1.2 with the majority of values ranging between 0.9 and 1.1. The evolution of the friction coefficient over the load cycles is not shown. For each test only one value for the coefficient of friction is presented. In an additional test, the vertical load was increased from 0.5 kN to 1.25 kN. Due to technical problems, the results obtained for 0.5 kN have to be interpreted very carefully. The remaining results are in accordance with the previous tests. Via an estimation of the contact area, it was calculated that the tests took place in a range of contact pressures between 30 MPa and 53 MPa. This is a much higher stress regime than reported in other works on railway ballast. While stresses at field conditions are hard to access, in laboratory tests on railway ballast [5,8,15,17,19] all applied stresses are clearly below 1 MPa.

In this work, cyclic friction tests were conducted on railway ballast. Two different types of ballast were investigated to check on possible differences. The applied vertical load was incrementally increased after a certain number of cycles. Compared to [25], much lower vertical loads were applied, aiming at investigating friction at a lower stress regime. Some of the tests involved scanning the ballast stones before the load increase to calculate the contact area. This allowed the stress at the contact to be estimated and thus an investigation on stress-dependency of the coefficient of friction and wear to be carried out. The obtained results were discussed regarding their effect on the DEM simulation of railway ballast.

All generated measurement data is openly available at the zenodo.org repository, see [26].

2. Experiments and data postprocessing strategies

Cyclic friction tests of two different types of railway ballast, Calcite and Kieselkalk, were conducted. For these tests, an angular specimen (stone with a distinctive tip) was sheared over a flat specimen. The cyclic friction tests involved a loading phase up to a specified vertical load, shearing at constant velocity over a 10 mm shear distance and an unloaded return to the initial contact point. In this way, a given number of cycles were run for a specified vertical load. Then, the vertical load was increased and the testing continued until the cycling was finished at the highest vertical load.

Table 1
Median roughness values, S_q (Root-Mean-Square height of selected area), of natural and sand blasted ballast specimen.

S_q [μm]	Calcite	Kieselkalk
Natural surface	53.8	35.7
Sand blasted	14.1	18.6

The following subsections contain details regarding the specimen preparation, the measurement equipment used, the two tested ballast types and the test procedures. Moreover, the postprocessing of the measured data is explained.

2.1. Material and specimen preparation

In this work, two different types of railway ballast were considered: Calcite (from Croatia) and "Kieselkalk", also known as Helvetic Siliceous Limestone, (from Switzerland). Please note that the Calcite ballast does not consist of the mineral calcite: $CaCO_3$.

Ballast stones with distinctive tips were chosen for the angular specimens, and larger stones were chosen to be made into the flat specimens. The stones were cleaned under running water to remove any dust attached to the surface and washed with acetone to remove any grease from human handling and to allow the epoxy to adhere fully. Buehler EpoxiCure™ 2, two part epoxy resin was used to mount the specimens. The angular specimens were propped up by a small amount of plasticine when necessary so that the angular part pointed directly upwards. The flat specimens were fully submerged in the epoxy, then cut in half using a tile saw and sanded flat using a belt sander. The flat specimens were then sand blasted to remove any sawing scars and return a more uniform rough surface more representative of the original stone surface, while still being flat.

The roughness values, S_q (Root-Mean-Square height of selected area), were measured for the sand blasted surface of each specimen prior to any friction tests being performed. The median roughness values for these sandblasted surfaces are given in Table 1. In the same table, the median of S_q values for natural surfaces, calculated by the authors in [27], are given. It shows that the sand blasted surfaces are smoother than the natural ones: for Calcite the factor is approximately 4 for Kieselkalk it is 2. However, it is assumed that roughness values change immediately after starting the test on both sides. Thus, these differences are not considered as relevant.

Pictures of generated specimens for both types of ballast considered, Calcite and Kieselkalk, are shown in Fig. 1.

2.2. Frictional testing equipment

UMT-3 (Universal Mechanical Tester) and UMT-2 machines made by Bruker were used for the mechanical friction testing. The UMT is an extremely versatile piece of mechanical testing equipment, with a modular design it can be set-up to perform a wide range of movements. The test set-up involved the linear stage with a DFH-20 load cell and a medium suspension attached to a specifically made vice to hold the specimens. The DFH-20 load cell used has a range of 0.2 N to 200 N and a resolution of +/− 0.001 N. The measured and controlled quantities are specified in Table 2.

The UMT device with mounted specimens is shown in Fig. 2.

As mentioned before, the friction tests were cyclic. At the beginning of the cycle, the specimens were loaded to the specified vertical load F_n. Then, the lower drive with the installed flat specimen was sheared at constant vertical load and at constant tangential velocity, $v_x = 1$ mm/s, for a shear distance of 10 mm. The cycle concluded with unloading the specimens and return of the lower drive to its initial position. In this way, a given number of cycles was conducted for a specified vertical load. Next, the vertical load is increased and the testing continues until the cycling is finished for the highest vertical load. A low shear velocity

(a) Calcite samples: angular and flat specimen

(b) Kieselkalk samples: two angular specimens

Fig. 1. Pictures of Calcite and Kieselkalk samples.

Table 2
Measured and controlled quantities at Universal Mechanical Tester (UMT) test rig. Measured data is sampled at a rate of 100 Hz.

Measured quantities		Cntr.
Vertical force	F_n	x
Tangential force	F_t	
Vertical (slider) position	z	
Tangential (lower drive) position	x	
Vertical (slider) velocity	v_z	
Tangential (lower drive) velocity	v_x	x
Coefficient of friction	$CoF = \frac{F_t}{F_n}$	

(a) UMT device with labeled components

(b) UMT during measurement

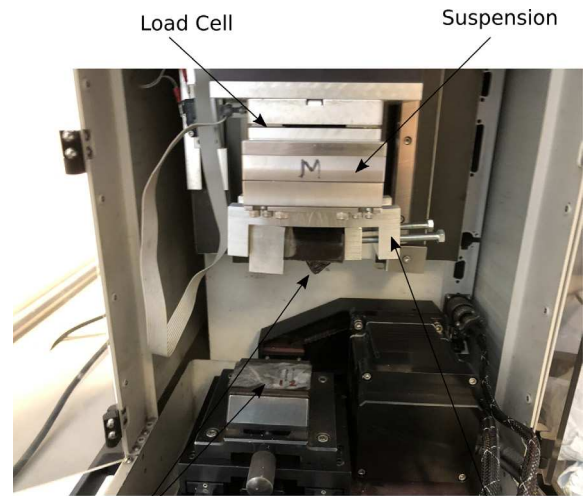**Fig. 2.** Used UMT device with mounted specimens.

is chosen for the tests to avoid any temperature related effects, which are assumed to play no role under field conditions.

In the experiments presented here, an angular specimen was always sheared over a flat specimen (prepared as described above). Therefore, it was sufficient to calculate the coefficient of friction CoF as simple division of tangential force by vertical force. In [25], angular stones were sheared over an uneven stone surface and a geometrical correction for the calculation of the CoF was introduced. As flat stone surfaces are used in this study, the application of this geometrical correction is not necessary. Moreover, the usage of a flat surface allows the study of the frictional behaviour exclusively, avoiding any form closure effects.

2.3. 3D scans and roughness measurements

Before and after the friction tests, 3D scans of the specimen were taken, both of the angular and the flat stone. As it will be described later, some test protocols included 3D scans before the applied vertical load was increased. The 3D scans are used for estimating the contact area between the specimens (from the angular specimen) and also to obtain the initial surface roughness of the flat specimen.

For this purpose, an Alicona InfiniteFocus SL was used, a non-contact imaging and measuring tool made by Alicona Imaging in Austria. It is able to take relatively fast, high resolution scans in 3D, allowing characteristics such as surface roughness and geometry to be calculated. The 5x optical lens was used for the scanning of all of the ballast stones, although 10x and 20x lenses were available for macro, micro and nano (up to 10 nm) scale measurements.

The Alicona device is able to calculate several quantities over the scanned region using built-in software. From the available options, only the roughness (Root-Mean-Square height of selected area), S_q, was used in this work.

Fig. 3 shows the Alicona scanning a flat specimen and as well as a flat specimen after friction testing.

2.4. Overview of load cases

Three different UMT test series were carried out with both ballast types. An overview is given in Table 3. Each experiment started with a fresh pair of stones. Five different vertical loads were investigated (10 N, 25 N, 50 N, 75 N and 100 N). Experiments with one and 100 cycles per vertical load have been carried out. Some test protocols included Alicona Scans before each increment of vertical load, this is indicated in Table 3 as well.

2.5. Calculation of contact area from 3D scans

Based on the 3D geometry data from the Alicona scans, the contact area between the stones was calculated. The idea is to look at the 3D mesh and to manually choose a small area in the flattened part of the

Table 3
Overview of tests. Each test started with a fresh pair of stones.

	Test	Type of stone	Scan	F_n	Cycles	Scan	F_n	Cycles	Scan	F_n	Cycles	Scan	F_n	Cycles	Scan	F_n	Cycles	Scan
									Test protocol									
Test series 1	KK1	Kieselkalk	S	10 N	100	S	25 N	100	S	50 N	100	S	75 N	100	S	100 N	100	S
	C1	Calcite	S	10 N	100	S	25 N	100	S	50 N	100	S	75 N	100	S	100 N	100	S
Test series 2	C2	Calcite	S	10 N	100					50 N	100					100 N	100	S
	C3	Calcite	S	10 N	100					50 N	100					100 N	100	S
	C4	Calcite	S	10 N	100					50 N	100					100 N	100	S
	KK2	Kieselkalk	S	10 N	100					50 N	100					100 N	100	S
	KK3	Kieselkalk	S	10 N	100					50 N	100					100 N	100	S
	KK4	Kieselkalk	S	10 N	100					50 N	100					100 N	100	S
Test series 3	C5	Calcite	S	10 N	1	S	25 N	1	S	50 N	1	S	75 N	1	S	100 N	1	S
	C6	Calcite	S	10 N	1	S	25 N	1	S	50 N	1	S	75 N	1	S	100 N	1	S
	C7	Calcite	S	10 N	1	S	25 N	1	S	50 N	1	S	75 N	1	S	100 N	1	S
	KK5	Kieselkalk	S	10 N	1	S	25 N	1	S	50 N	1	S	75 N	1	S	100 N	1	S
	KK6	Kieselkalk	S	10 N	1	S	25 N	1	S	50 N	1	S	75 N	1	S	100 N	1	S
	KK7	Kieselkalk	S	10 N	1	S	25 N	1	S	50 N	1	S	75 N	1	S	100 N	1	S
	KK8	Kieselkalk	S	10 N	1	S	25 N	1	S	50 N	1	S	75 N	1	S	100 N	1	S
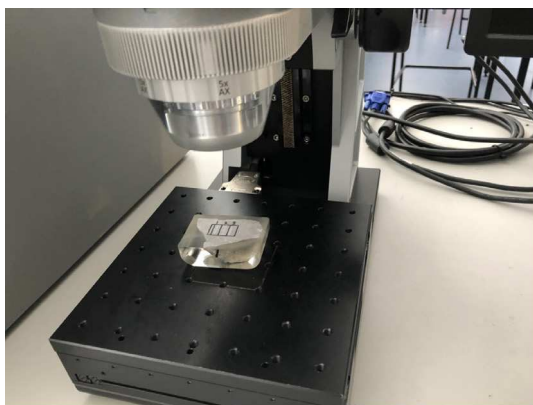
(a) Alicona scanning a flat specimen

(b) flat specimen after friction testing, including wear scar

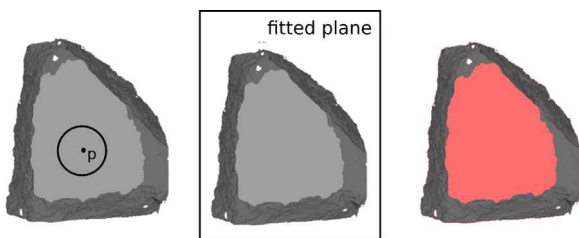**Fig. 3.** Alicona device and flat specimen after testing.

Fig. 4. Example of area estimation method. (For interpretation of the references to colour in this figure legend, the reader is referred to the web version of this article.)
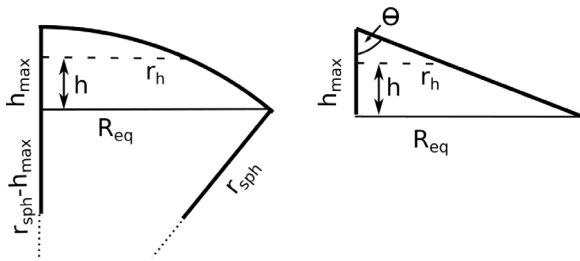
stone. Then, a plane is fitted through this area and all points with a low normal deviation from this fitted plane are considered to be part of the contact area. In more detail, the method used is described below and is also visualised in Fig. 4.

1. pick a point p on the contact area (left part of Fig. 4).
2. specify a radius r
3. choose all points with distance smaller than r (circle in left part of Fig. 4)
4. fit a plane (least squares) through these points (middle part of Fig. 4)
5. for all points of the mesh: calculate distance between plane and point
6. contact area points = all points whose distance to plane is smaller than a threshold l
7. contact area = sum the area belonging to these points (red in the right part of Fig. 4)

Clearly, the contact area obtained will depend on the point p and also on the two parameters r and l. As with any evaluation methodology, an error will always be made, but cannot be specified easily. In the openly available dataset, [26], the used parameters p, r, l and the calculated contact areas are given.

2.6. Calculation of the change of specimen height over cycles

As already described above, the UMT device measured the x and z coordinate of the upper stone during the test. For test series 1 and 2, this data is used to calculate the change of the specimen's height over the test cycles. For each cycle, the measured z coordinate is interpolated at the middle of the shear distance and assigned as height value for this cycle, h_n. The height change is then the difference in height for the following cycles, $h = h_{n+1} - h_n$. When the vertical load was increased in the test protocol, there was a jump in the height values, even if specimens were not removed from the test rig for scanning and put back in (due to elasticity effects). These jumps are removed, such that continuous curves are obtained. For this reason, no height change can be computed for test series 3, where only one cycle per vertical load level is conducted.

2.7. Estimating contact area development over cycles

For test series 1 and 2, a method to estimate the contact area per cycle was developed. This information will be used later for an estimation of contact pressure per cycle and for the wear analysis.

The idea was to use the calculated height change over the cycles, h, together with the calculated contact area at the end of the test protocol, $A(100N)$. Two assumptions regarding the shape of the worn

Fig. 5. Drawing of spherical cap and cone fitting.

Test	C2	C3	C4	C5	C6	C7
S_q [µm]	10.9	13.7	14.3	18.8	15.5	13.9
Test	KK2	KK3	KK4	KK5	KK6	KK7
S_q [µm]	16.4	18.5	7.4	29.8	19.9	18.8

tip are made: a spherical cap and a cone are fitted as explained below. From $A(100N)$ an equivalent radius, R_{eq} is calculated both for the spherical cap and cone fitting. Fig. 5 shows a schematic drawing and the nomenclature. Eqs.(1) are used to estimate the development of contact area assuming a spherical tip shape. Here, h_{max} denotes the maximal height change (at the end of the test), r_{sph} the radius of the fitted sphere, r_h the radius of the contact area over the cycles and A_{est}^{sph} the obtained estimated contact area under the assumption of a spherical cap.

$$A(100N) = \pi R_{eq}^2 \qquad \Leftrightarrow R_{eq} = \sqrt{\frac{A(100N)}{\pi}} \qquad (1a)$$

$$r_{sph}^2 = R_{eq}^2 + (r_{sph} - h_{max})^2 \qquad \Leftrightarrow r_{sph} = \frac{R_{eq}^2 + h_{max}^2}{2 h_{max}} \qquad (1b)$$

$$r_h^2 = r_{sph}^2 - (r_{sph} - h)^2 \qquad \Rightarrow A_{est}^{sph} = \pi r_h^2 \qquad (1c)$$

Analogously, Eqs. (2) are used assuming a conical tip shape. Here, θ denotes the opening angle of the cone and A_{est}^{cone} the obtained estimated contact area under the assumption of a cone.

$$A(100N) = \pi R_{eq}^2 \qquad \Leftrightarrow R_{eq} = \sqrt{\frac{A(100N)}{\pi}} \qquad (2a)$$

$$\tan(\theta) = \frac{R_{eq}}{h_{max}} \qquad (2b)$$

$$r_h = h \tan(\theta) \qquad \Rightarrow A_{est}^{cone} = \pi r_h^2 \qquad (2c)$$

The explained methodology will be validated in Section 3.5.

2.8. Wear behaviour

For the analysis of the wear behaviour, the required equations are introduced in this subsection. The wear volume can be calculated as a function of the number of cycles for test series 1 and 2. Here, again the shapes of spherical cap and cone are assumed for the stone's tip,

$$V_{sph} = \frac{1}{6} \pi h \left(3 r_h^2 + h^2\right) \qquad (3)$$

$$V_{cone} = \frac{1}{3} \pi r_h^2 h \qquad (4)$$

compare the previous subsection for the notation.

The classical Archard's law, see [28], assumes a relation between the change in volume, ΔV, and the length of the shear distance, Δx:

$$\Delta V = \frac{K}{H} F_n \Delta x, \qquad (5)$$

where F_n is the applied normal load, K is a constant and H is the hardness of the considered material.

Often, an adapted Archard law is used, where wear volume and normal force are replaced by wear depth and contact pressure, respectively:

$$\Delta z_w = \frac{K}{H} p \Delta x, \qquad (6)$$

where z_w denotes wear depth and p contact pressure. This is a useful formulation in the case of non-constant normal stress distributions

within the contact patch. However, in the current study, only mean contact pressures (constant) are considered. Thus, both formulations are equivalent. Therefore, only the classical Archard's law will be considered.

In a dissipated energy based approach, compare [29,30], the change in volume, ΔV, is proportional to the dissipated energy:

$$\Delta V = c \Delta W, \qquad (7)$$

where c is a constant. The cumulated dissipated contact energy (frictional work) can be calculated as function of the conducted cycles,

$$W = \sum_{cycles} F_n \operatorname{CoF} \Delta x. \qquad (8)$$

Both approaches will be compared using the measured values of height change and computed volume change to see whether the assumption of constant wear law coefficients (K, H, c) is valid.

3. Results

3.1. Coefficient of friction: CoF

To get a first impression of the CoF values obtained, Fig. 6 shows results for the test C1 carried out with Calcite. The CoF is plotted over the shear distance and number of cycles for the different vertical loads. A scatter of the data can be observed, which is stronger for lower vertical loads and then reduces with increasing vertical load. In most of the experiments, lower CoF values were measured during the first cycles at a given vertical load. This effect is more pronounced at lower vertical loads. For further analysis, one CoF value is calculated for each cycle from the measured test data. To do so, the median of the values between 2 and 8 mm shear distance is taken. Fig. 7 shows the development of the CoF values plotted over the cycles for all three test series.

3.2. Roughness

Based on the 3D data gained from the Alicona scans, roughness was analysed for Calcite and Kieselkalk stones from test series 2 and 3 to see, if the scatter of the CoF data and the variations in roughness might be related. All roughness measurements have been done at the flat stone before starting the UMT experiment. The results are summarised in Table 4 showing that most of the investigated stones have similar S_q values.

3.3. Contact area calculated from 3D scans

For test series 1 and 3, Alicona scans were always taken after the last cycle with a given vertical load, i.e. scans are taken after the 100th cycle for test series 1 and after one cycle for test series 3. For test series 2, only at the start and the end of the test protocol Alicona scans were taken, compare Table 3. The contact area is estimated based on the approach described in Section 2.5.

Fig. 8 shows the development of the contact area for the test KK8. The tips of the stones were each time positioned manually for scanning with the Alicona device, which caused a variation in the amount of the
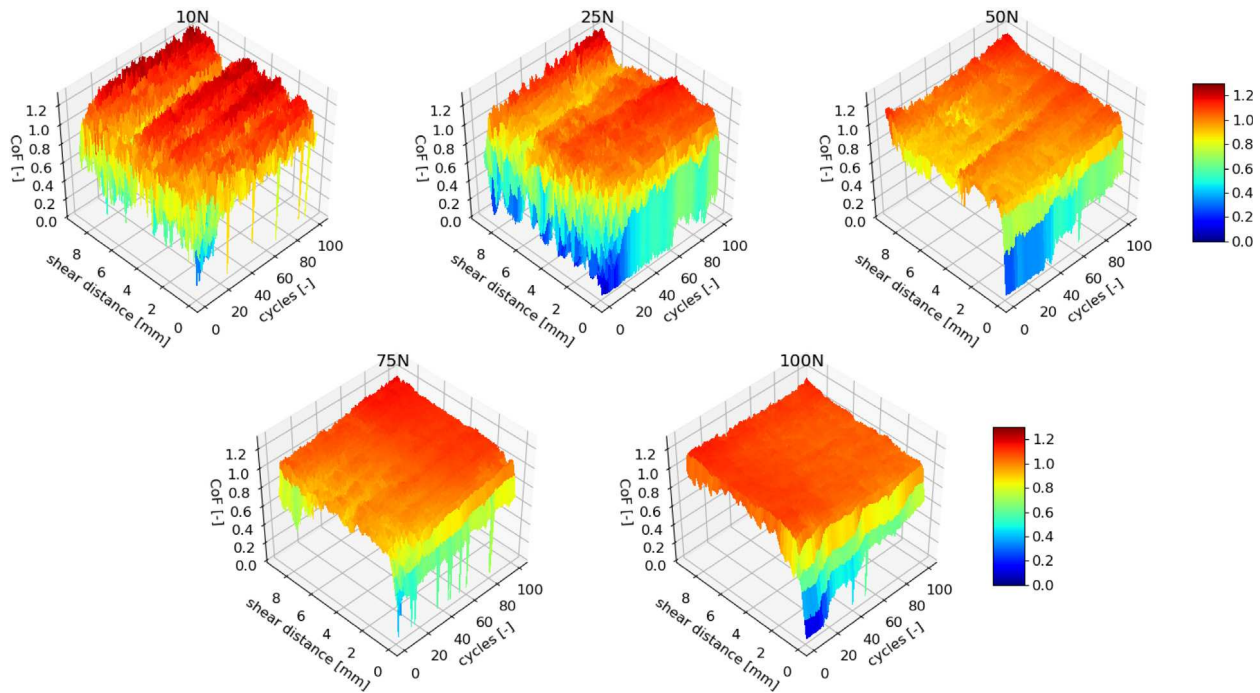
Fig. 6. CoF dependent on number of cycles and shear distance. Results are shown for Calcite test C1 for all vertical loads.

scanned surface, e.g. at 25 N the scanned surface is larger than at 10 N. As long as the contact area is included in the scanned surface, this is not important. In Fig. 8, the calculated contact area is shown in red, and the fitting circle in magenta (compare step 3 in the calculation of contact areas in Section 2.5). The calculated contact area grows when the applied vertical load is increased. Due to the stone's geometry and the error resulting from the methodology to determine the contact area only a minor difference from 75 N to 100 N can be seen.

Fig. 9 shows the contact areas, calculated for all tests, plotted over the applied vertical force. As expected, there is a difference when comparing results for test series 3 with 1 cycle and test series 1 with 100 cycles because of the wear mechanism. Both investigated types of stone show a similar characteristic, but even more, also the quantitative values are very similar.

3.4. Evaluated height change

The height changes, calculated as described in Section 2.6, are plotted over cycles in Fig. 10 for test series 1 and 2. As test series 3 only had one cycle for each vertical load applied, no height changes can be calculated here. For both test series 1 and 2 the final height change is between 0.3 mm and 0.9 mm. The values obtained from test series 2 show considerably more scatter than the ones obtained from test series 1. No distinct difference between Calcite and Kieselkalk can be seen. Both types of ballast show mostly a similar behaviour: after an increase of the vertical load the height change grows strongly and this growth reduces with the number of cycles under constant vertical load.

3.5. Estimated contact area development over cycles

Fig. 11 shows the development of the contact area dependent on the number of cycles, calculated as described in Section 2.7 together with measurement results derived from the Alicona scans. The measurement results are in good agreement with the results for the spherical stone cap. Furthermore, this plot reveals the non-linear relationship between number of cycles and the development of the contact area. The contact area increments decrease with increasing number of cycles as long as the vertical force is kept constant. Whenever the vertical force is

increased (after every 100 cycles) an increase of the area increments is predicted.

As the assumption of the spherical cap fits much better to the measured data of test series 1, the spherical cap is used to estimate the contact areas for test series 2. Using the same methodology, the development of the estimated contact area over the cycles is shown in Fig. 12 for test series 2.

3.6. Wear

As seen in the previous subsection, the development of the estimated contact area (assuming a spherical cap) looks very similar for Calcite and Kieselkalk stones. This is an indication that also the wear resistance (volume loss) might be very similar, but this cannot be concluded directly from the contact area results.

Using Eq. (3) the wear volume is calculated assuming a spherical cap and plotted over the conducted cycles in Fig. 13. For comparison, also Archard's law, Eq. (5) is evaluated (with K/H chosen such that the volume coincides at the end of the test). Moreover, the dissipated energy is calculated from Eq. (8). In Fig. 14, the wear volume is plotted over the dissipated energy together with model predictions for the dissipated energy based approach (dea) according to Eq. (7). Finally, Fig. 15 shows the contact pressure over the test cycles, for improved visibility, values are shown up to 100 N/mm². For the tests C1 and KK1 the development of the wear volume is plotted on a second y-axis in Fig. 15(a). For the remaining tests, the wear volume is not plotted, as this would decrease the plots' readability strongly.

4. Discussion

The results presented so far will be discussed in the following subsections. The results obtained for the coefficient of friction are discussed in Section 4.1. In Section 4.2 a wear analysis is carried out. Finally, the relevance of the CoF testing results for DEM simulations are discussed in Section 4.3.
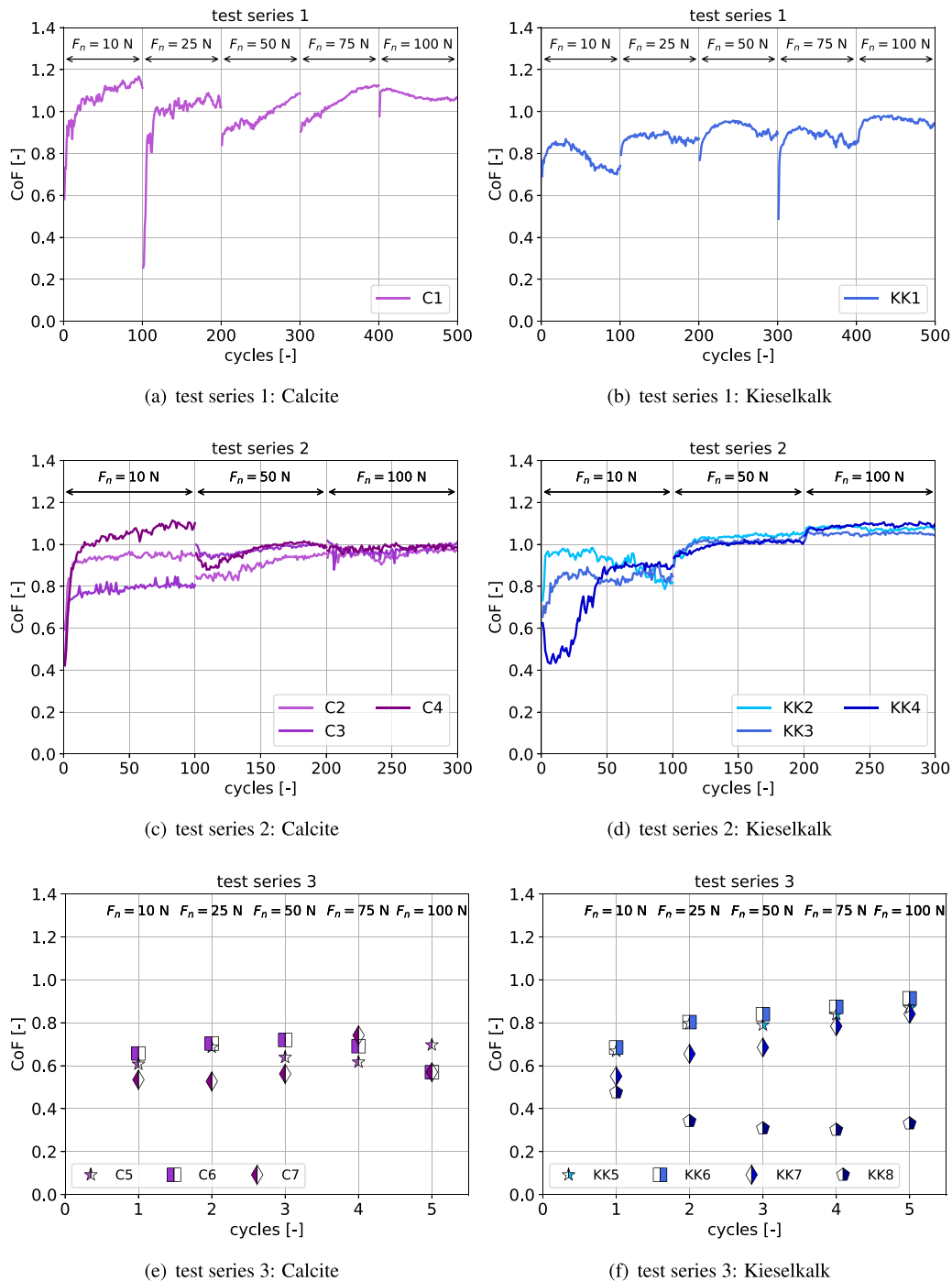
Fig. 7. CoF plotted over cycles for both Calcite and Kieselkalk for test series 1, 2 and 3.

4.1. CoF

All measured CoF values are summarised in Fig. 7 and three main observations can be made. First, when comparing Calcite and Kieselkalk no clear difference can be seen between the measured CoF values. Second, there is a high scatter in the measurements. Third, in test series 1 and 2, which included 100 cycles for each level of vertical load, higher CoF values were measured than in test series 3, where only one cycle per vertical load was conducted.

When comparing both types of ballast, in test series 1 higher CoF values are measured for Calcite than for Kieselkalk. For test series 2 and 3, Kieselkalk shows higher CoF values than Calcite for vertical loads above 50N.

To identify possible sources of the scatter in the tests, the initial roughness values S_q before starting the UMT tests were checked. All values were in a similar range, thus, variations in roughness are obviously not the only reason for the observed scatter. As stones are a natural material non-homogeneous composition or the stone's geometry might be a reason, but also effects from the UMT control system. This is in agreement with the fact that higher scatter was observed at tests with low loads (10 N) where also a higher relative error of the controlled vertical load was seen.

In test series 1 and 2, 100 cycles are conducted for each level of applied vertical load. Thus, different mechanisms will be active compared to test series 3 with only one cycle. For test series 1 and 2, the measured CoF value of the first cycle of an applied vertical
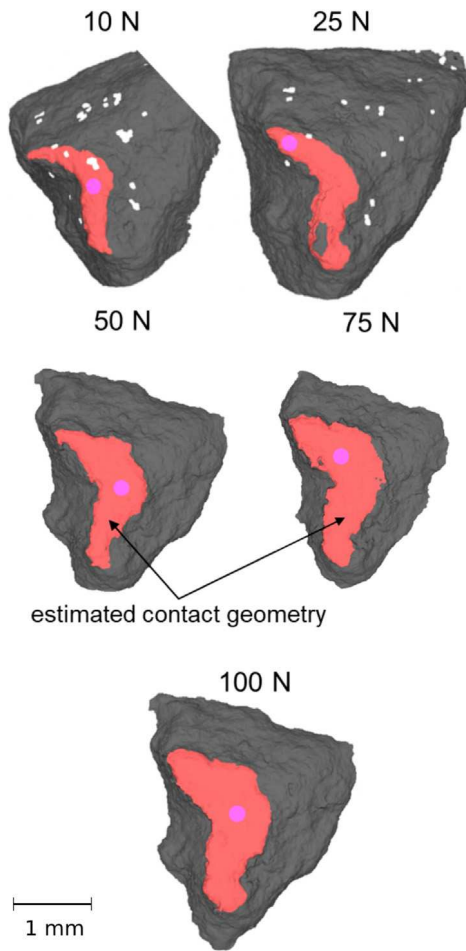
Fig. 8. Example for the development of the contact area (red) for test KK8. (For interpretation of the references to colour in this figure legend, the reader is referred to the web version of this article.)

(a) Calcite

(b) Kieselkalk

Fig. 9. Development of the contact area as a function of vertical load for Calcite and Kieselkalk.

load is always lower than the value for the 100th cycle, as shown in Fig. 7. This effect is more pronounced for tests with 10 N vertical load than for tests with 100 N. A possible explanation for this behaviour includes the contact pressure. In this study, always the mean contact pressure, applied normal load divided by contact area, is considered. At the beginning of the test, high contact stresses are present, which decrease when the initial tip of the ballast stone is flattened. In Figs. 11 and 12 most tests show a fast increase of the estimated contact area in the first cycles, which corresponds to a drop in contact pressure. With continued cycling, the contact surfaces are conditioned as wear takes place and the contact area grows more slowly. This process repeats with every increase in vertical load. In tribology, it is a known phenomenon that some materials have a stress dependent CoF, i.e. the CoF reduces with increasing contact vertical stress, see [22,23,31–35]. Fig. 16 shows the contact stress and CoF for the first cycle (higher contact stress) and last cycle (lower contact stresses) of an applied vertical force for both Calcite and Kieselkalk, indicating a stress-dependency of the CoF for the investigated ballast types. However, there exist also facts contradicting this hypothesis. From the last cycle of an applied vertical load to the first cycle of the increased vertical load, contact stress will increase. This is plotted in Fig. 17 together with the corresponding CoF. While for Calcite the measured CoF mostly drops with an increase in stress, for Kieselkalk most of the results show a slight increase of the CoFs with increasing contact stresses. However, even though there are some indications that the CoF depends on contact pressure, a final conclusion is still hard to draw because of the following reasons. First, there is
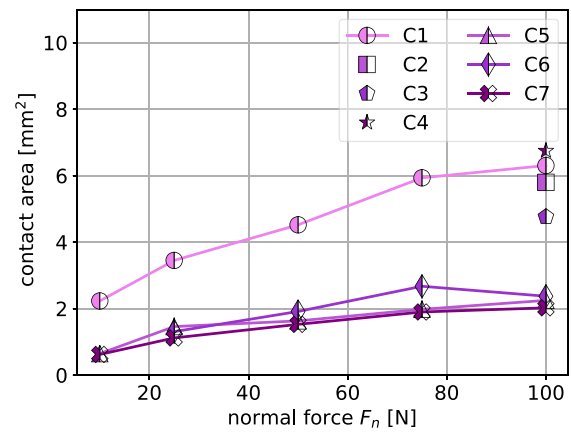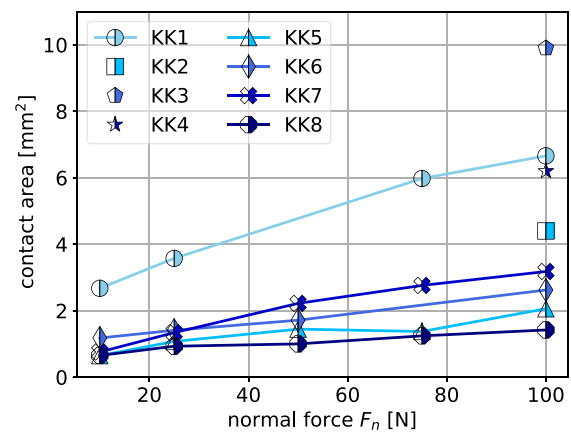
an overlaying of two tribological mechanisms mentioned earlier — stress-dependency of CoF and conditioning of the surfaces. Second, there is a strong scatter of the measured CoF values probably caused by differences in the stone's geometry and highly non-homogeneous material composition and also affected by the UMT control system. More tests, possibly at lower contact stresses, would be needed for a better separation of these two tribological mechanisms.

In test series 3, only one cycle per applied vertical load was conducted. For Calcite, the measured CoF values, ranging between 0.5 and 0.8, are considerably lower than those measured in test series 1 and 2. For Kieselkalk the measured CoF values increase with increasing vertical load, approaching similar values as those measured in test series 1 and 2. This is with the exception of test KK8, which shows a decreasing trend in the CoF and also consists of the lowest CoF values measured in the whole measuring campaign. No obvious explanation for the different behaviour of this test exists.

Regarding the cyclic test series 1 and 2, the measured CoF values after 100 cycles are in the same range as those observed in [25]. This is surprising, as in [25] different ballast was considered and a much higher vertical load, 1 kN, was applied. Nevertheless, the measured CoF values after 100 cycles from Fig. 7 range between 0.8 and 1.2, which is nearly identical with the results found in [25].
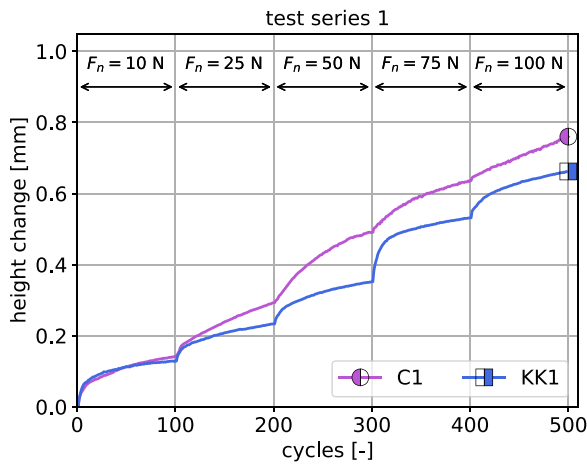
(a) test series 1: Calcite and Kieselkalk
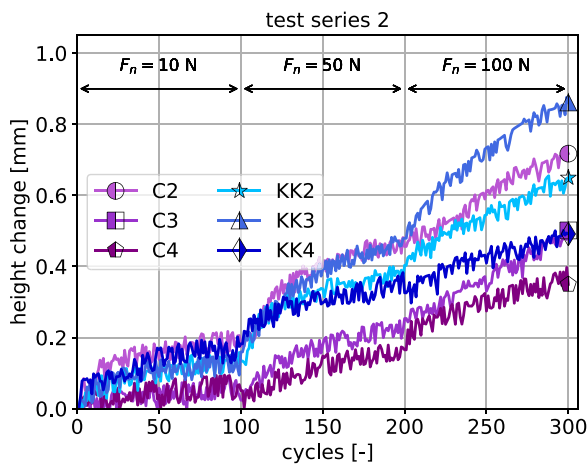
(b) test series 2: Calcite and Kieselkalk

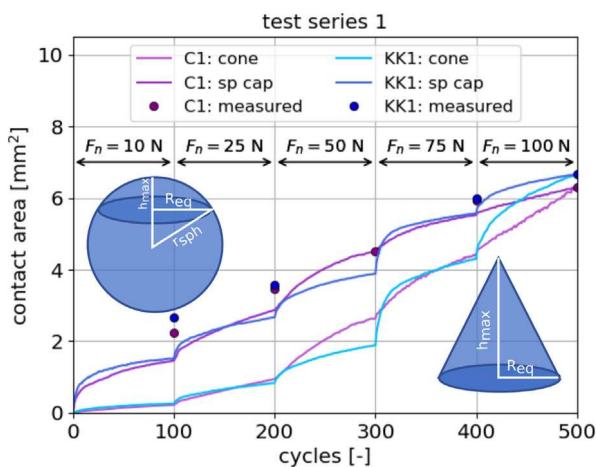**Fig. 10.** Calculated height change plotted over cycles for test series 1 and 2.

Fig. 11. Development of the estimated contact area dependent on the number of cycles for tests series 1. Results according to an assumed spherical and conical shape of the tip of the stone together with measurement results derived directly from the 3D scans.
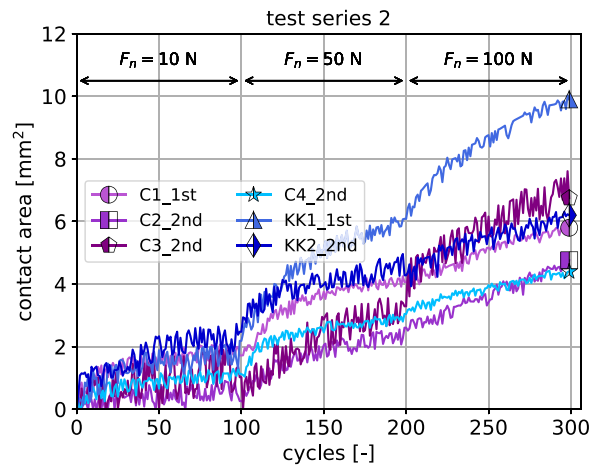

Fig. 12. Development of the estimated contact area, A_{est}^{sph}, dependent on the number of cycles for tests series 2 under the assumption of spherical cap.

4.2. Wear behaviour

The wear volume curves in Figs. 13 and 14 confirm that the wear resistance of Calcite and Kieselkalk is very similar in the considered experiments. Only test KK3 shows a higher wear volume, while all other tests end with a wear volume between 1 mm^3 and 2 mm^3.

According to the contact area results, increased wear volume increments can be observed at the first cycles when the vertical load is increased. The fitted Archard's law in Fig. 13 is piecewise linear, while the calculated wear volume shows a non-linear characteristic. The overall trend is described well by Archard's law, but the non-linear behaviour cannot be reproduced. The same is true for the relationship between dissipated energy and wear volume, calculated in Fig. 14 from measured values and from the modelling approach in Eq. (7). Thus, both wear modelling approaches describe the general trend, but do not reproduce the observed non-linearities (under the assumption of constant wear law coefficients). Fig. 15 shows the calculated development of the mean contact pressure (for improved visibility, values are shown up to 100 MPa). A direct comparison between contact pressure and wear volume can be seen in Fig. 15(a) for tests C1 and KK1. For the remaining tests, this data is not plotted in one Figure (reduced readability), but can be obtained from combining Figs. 13 and 15. Increasing the load results in an immediate increase of the mean contact pressure. During the following cycles at a constant vertical load the mean contact pressure is reduced again because of the growing contact area resulting from wear. It is clear that the increased wear volume increments at the first cycles after load increase correspond to a higher contact pressure. This is an indication that the coefficients in the wear laws might be pressure dependent. To further investigate this possibility, the measured height values for tests C1 and KK1 were smoothed applying a central moving average of width $N = 9$. The smoothing was applied to each level of applied vertical load separately. The first $(N-1)/2$ values remained unchanged, while the last $(N-1)/2$ values were continued constantly. From the smoothed height values, smoothed wear volume increments and contact pressures were calculated. Without the smoothing process, the wear volume increments would have scattered strongly. From the smoothed data, the local wear coefficients were calculated both from Archard's law (5) and the dissipated energy based approach (7). These wear coefficients are plotted over the contact pressure in Fig. 18 for the tests C1 and KK1. Both wear coefficients have the same unit and show a similar behaviour: When the vertical load is increased, the contact stress is highest, which corresponds also to the highest values of the wear coefficients K/H and c. When the cycling continues, the contact pressure reduces and so do the wear coefficients. For increased visibility, only contact pressures up to 20 N/mm^2 are
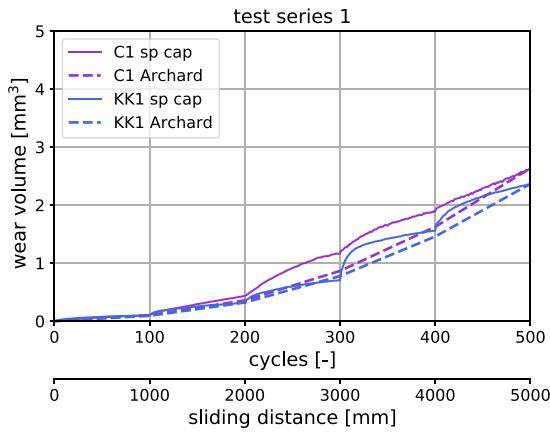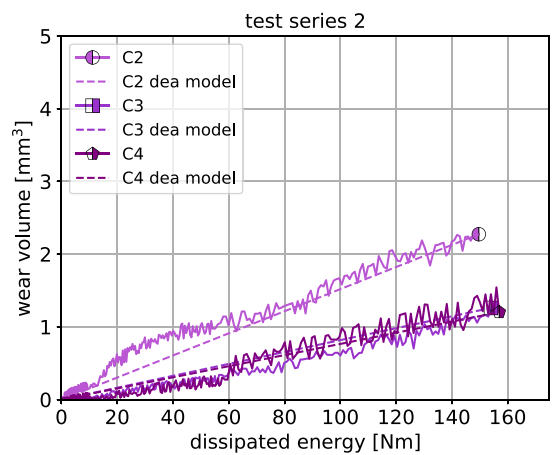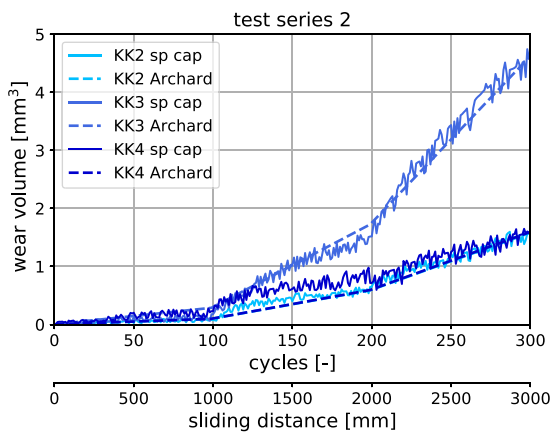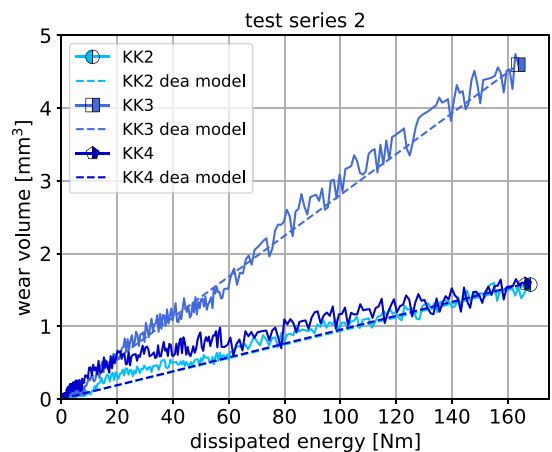
(a) test series 1
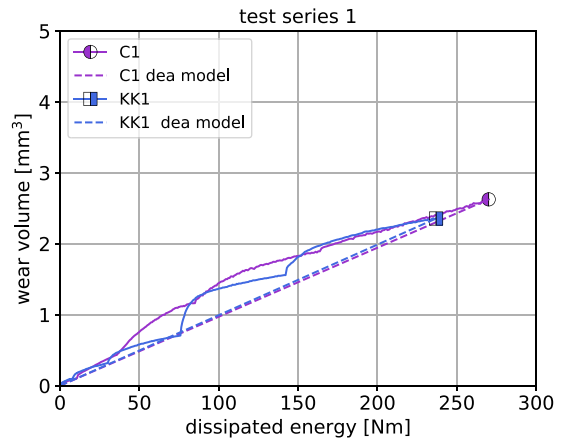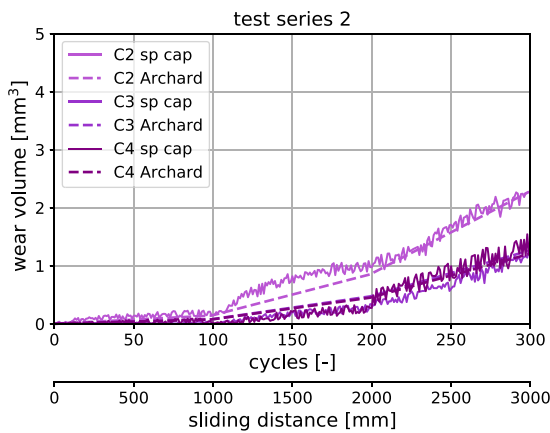
(b) test series 2: Calcite
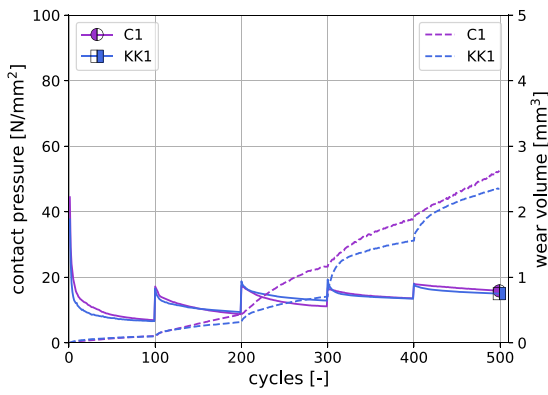

(c) test series 2: Kieselkalk

Fig. 13. Development of wear volume over test cycles (second *x*-axis shows sliding distance) for tests series 1 and 2. Results according to an assumed spherical cap shape of the tip of the stones and Archsard's law.

(a) test series 1

(b) test series 2: Calcite

(c) test series 2: Kieselkalk

Fig. 14. Development of wear volume dependent on cumulated dissipated contact energy for tests series 1 and 2. Results according to an assumed spherical cap shape of the tip and dissipated energy approach (dea) model, (7).

shown (cutting values from the F_n =10 N tests). The plot in Fig. 18 supports a pressure dependency of the wear coefficients. Furthermore, it can be seen that from the conducted measurements, similar values were calculated for K/H and c: the formulas for the wear coefficients differ only in the coefficient of friction, and CoF values in the conducted tests were approximately 1. This explains why Archard's law and the dissipated energy based approach have similar local wear coefficients
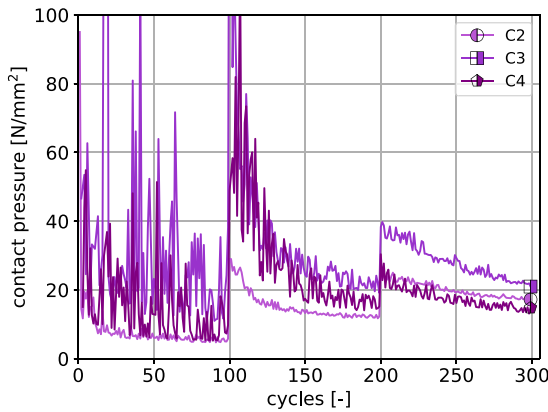
for these tests. For CoF values different from 1, clear differences in the local wear coefficients will occur.
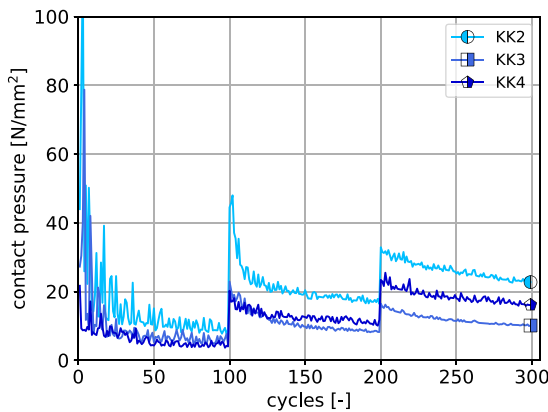
In [36], tests on wear resistance according to the European standard EN 1097-1 and EN 13450 (Annex E) were carried out for the same
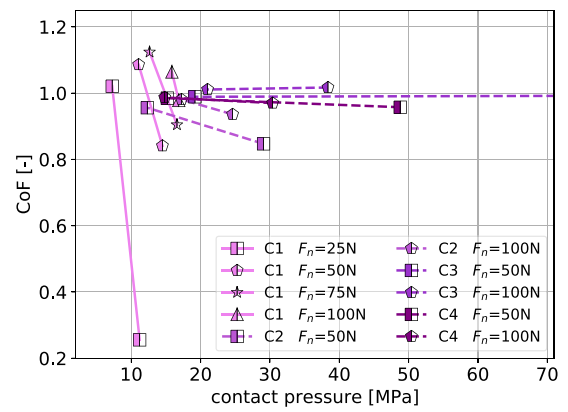
(a) test series 1
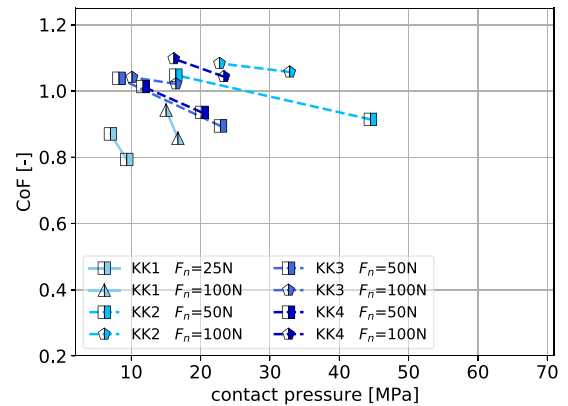

(b) test series 2: Calcite

(c) test series 2: Kieselkalk

Fig. 15. Development of mean contact pressure over test cycles for tests series 1 and 2. Results according to an assumed spherical cap shape of the tip. For test series 1, also the wear volume is shown for comparison.

(a) Calcite

(b) Kieselkalk

Fig. 16. Median CoF of the first (higher contact pressure) and 100th cycle (lower contact pressure) at the considered vertical load – connected with solid and dashed lines – for Calcite and Kieselkalk plotted over the mean contact pressure.

4.3. Relevance for DEM simulations

When looking in the literature, CoF values in the range of 0.4 to 0.8 are typically used for DEM simulations of railway ballast, [3–19]. In the experiments presented in this work, this range is mainly covered by the results for tests series 3 with only one cycle (higher contact pressures). In test series 1 and 2, the measured CoF values where (almost all) higher than 0.8 after a few cycles. When looking to ballast in real track, millions of load cycles occur. Here, higher CoF values may exist according to the findings in this work.

The relatively low values used in DEM simulations – 0.4 to 0.8 comparable to test series 3 – are not surprising. For parametrisation and validation of DEM models, direct shear tests or monotonic triaxial tests are frequently used, see e.g. [5,6,8,15,19]. In these tests, always fresh stones come into contact, which might be a comparable situation to test series 3. The calibrated DEM models are then used to simulate cyclic loading, e.g. in box tests [2,37], to investigate load cases closer to track conditions. In the cyclic loading in box tests or at track sites, contact partners stay mostly the same and are sheared repeatedly over each other. This scenario is quite similar to the cyclic friction tests of series 1 and 2, where CoF values between 0.8 and 1.2 were measured.

The above findings are a good motivation to develop more sophisticated friction and/or wear models for DEM simulations, especially for research focussing on the bulk behaviour of granular materials under cyclic loading.

types of ballast stones. Wear resistance is investigated using Micro-Deval tests, where ballast stones are turned inside a metallic cylinder together with water. In this highly dynamic test, wear comes not only from friction, but also from the impact after a free fall phase. In the conducted tests, Kieselkalk performed better compared to Calcite. The Mico-Deval tests differ considerably from the cyclic friction tests described in this work. Therefore, differences in the found wear behaviour between both testing methods are not surprising.
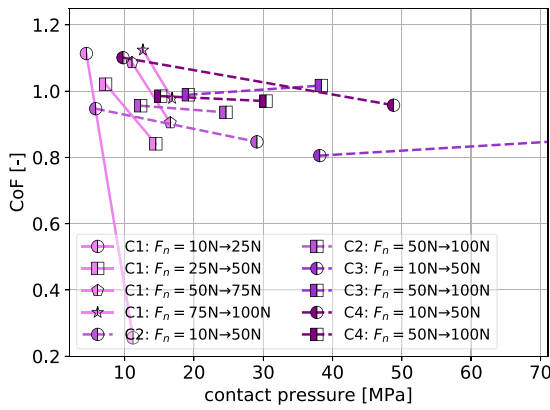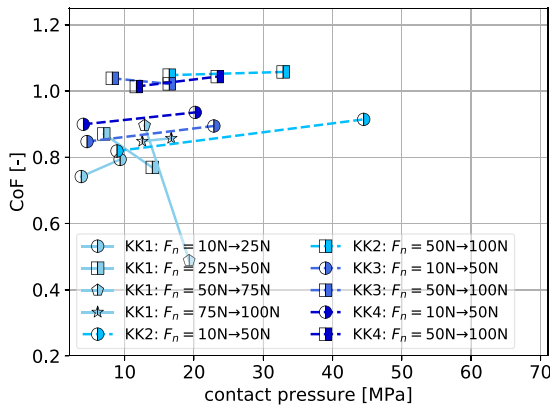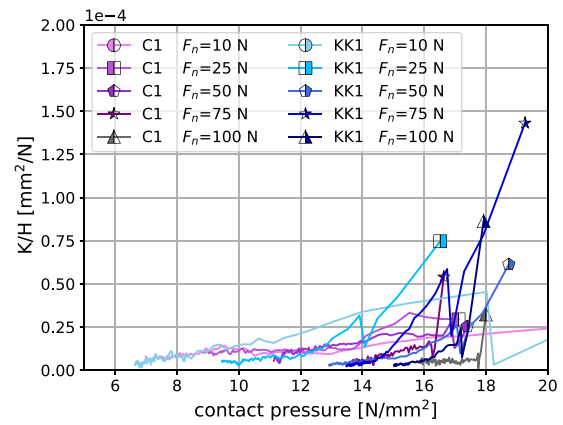
(a) Calcite

(b) Kieselkalk

Fig. 17. Comparison of the CoF of the 100th cycle at the vertical load (lower contact pressure) with the first cycle of the increased load (higher contact pressure) for Calcite and Kieselkalk plotted over the mean contact pressure.

(a) from Archard's law (5): $K/H = \Delta V / (F_n \Delta x)$

(b) from dissip. energy based approach (7): $c = \Delta V / (F_n \, \mathrm{CoF} \, \Delta x)$

Fig. 18. Wear coefficients from both Archard's law and the dissipated energy based approach plotted over contact pressure for tests C1 and KK1.
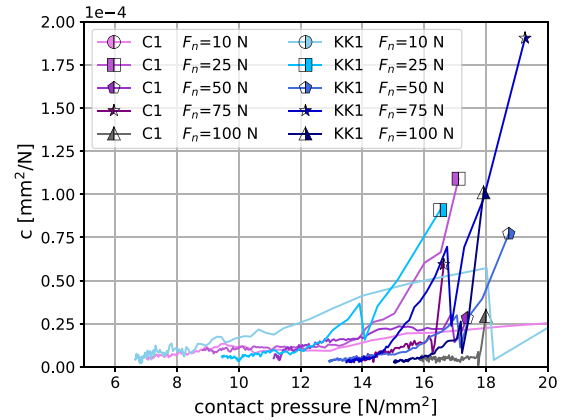
5. Conclusions

The frictional and wear behaviour of two types of railway ballast stones – Calcite and Kieselkalk – has been investigated at different vertical loads. Furthermore, 3D scans of the investigated stones have been carried out to get information about roughness, contact area, contact pressure and wear resistance. The following conclusions can be drawn from these investigations:

- The CoF measurements showed no obvious difference when comparing the two types of stone.
- The CoF values showed a considerable scatter for both types of stone. This scatter is not only caused by variations in roughness. It is expected that issues regarding the control of the vertical load contributed to the observed scatter. An indication for this is that the scatter was more pronounced at low vertical loads, where the control of the vertical load had a higher relative error. As stones are a natural material, variations in material properties can also contribute to the scatter of the measured CoF.
- Both types of stones showed lower CoF values during the first cycle at a given vertical load. This was more pronounced at lower vertical loads.
- In test series 3, (only one cycle per vertical load) and the measured CoF values ranged between 0.3 and 0.9. In test series 1 and 2, (100 cycles per vertical load) the measured CoF values were (after a few cycles mostly) in the range of 0.8 and 1.2.

- The range of CoF values typically used for DEM simulations of railway ballast (0.4 −0.8) are covered by the CoF values measured in non-cyclic test series 3 (only one cycle at a given load), while in cyclic tests higher values of the CoF were measured. Thus, more sophisticated friction models for DEM simulations are necessary, if both cyclic and non-cyclic shearing is to be simulated.
- There are indications that the CoF depends on contact pressure, but with some contradictions. These contradictions may result from the fact that different mechanisms acting in parallel are responsible for the development of the CoF, namely the stress-dependency of the material behaviour and conditioning of the surfaces (in the sense of roughness changes and contamination of the contact by wear debris) both influencing the CoF.
- Both types of stone showed a similar behaviour with respect to the development of contact area and wear volume (wear resistance).
- The wear volume, and related with this the contact area, show a non-linear relationship with the number of cycles and the cumulated dissipated contact energy, respectively. Both wear modelling approaches, Archard's law and the dissipated energy based approach describe the general trend. Under the assumption of constant wear law coefficients, they do not reproduce the observed non-linearities at the beginning of the experiment and the first cycles after increasing the vertical load. This is related to variations in the mean contact pressure. This knowledge is an important basis for improved wear laws to be used for example in DEM simulations of ballast focussing on scenarios with a high number of load cycles.

CRediT authorship contribution statement

Declaration of competing interest

The authors declare that they have no known competing financial interests or personal relationships that could have appeared to influence the work reported in this paper.

Data availability

The datasets generated and analysed during the current study are openly available in the zenodo.org repository, see [26].

Acknowledgements

References

[1] Cundall PA, Strack ODL. A discrete numerical model for granular assemblies. Geotechnique 1979;29(1):47–65. http://dx.doi.org/10.1680/geot.1979.29.1.47.

[2] Laryea S, Baghsorkhi MS, Ferellec J-F, McDowell G, Chen C. Comparison of performance of concrete and steel sleepers using experimental and discrete element methods. Transp Geotech 2014;1(4):225–40. http://dx.doi.org/10.1016/j.trgeo.2014.05.001.

[3] Li H, McDowell GR. Discrete element modelling of under sleeper pads using a box test. Granul Matter 2018;20(2):26. http://dx.doi.org/10.1007/s10035-018-0795-0.

[4] Kumar N, Suhr B, Marschnig S, Dietmaier P, Marte C, Six K. Micro-mechanical investigation of railway ballast behavior under cyclic loading in a box test using DEM: effects of elastic layers and ballast types. Granul Matter 2019;21(4):106. http://dx.doi.org/10.1007/s10035-019-0956-9.

[5] Ngo NT, Indraratna B. Improved performance of rail track substructure using synthetic inclusions: Experimental and numerical investigations. Int J Geosynth Ground Eng 2016;2(3):24. http://dx.doi.org/10.1007/s40891-016-0065-3.

[6] xi Miao C, jie Zheng J, jun Zhang R, Cui L. DEM modeling of pullout behavior of geogrid reinforced ballast: The effect of particle shape. Comput Geotech 2017;81:249–61. http://dx.doi.org/10.1016/j.compgeo.2016.08.028.

[7] Ngo NT, Indraratna B, Rujikiatkamjorn C. DEM Simulation of the behaviour of geogrid stabilised ballast fouled with coal. Comput Geotech 2014;55:224–31. http://dx.doi.org/10.1016/j.compgeo.2013.09.008.

[8] Qian Y, Mishra D, Tutumluer E, Kazmee HA. Characterization of geogrid reinforced ballast behavior at different levels of degradation through triaxial shear strength test and discrete element modeling. Geotext Geomembr 2015;43(5):393–402. http://dx.doi.org/10.1016/j.geotexmem.2015.04.012, Special issue on Geosynthetics for Transportation Applications.

[9] McDowell GR, Li H. Discrete element modelling of scaled railway ballast under triaxial conditions. Granul Matter 2016;18(3):1–10. http://dx.doi.org/10.1007/s10035-016-0663-8.

[10] Indraratna B, Ngo N, Rujikiatkamjorn C, Vinod J. Behavior of fresh and fouled railway ballast subjected to direct shear testing: Discrete element simulation. Int J Geomech 2014;14(1):34–44. http://dx.doi.org/10.1061/(ASCE)GM.1943-5622.0000264.

[11] Tutumluer E, Qian Y, Hashash YM, Ghaboussi J, Davis DD. Discrete element modelling of ballasted track deformation behaviour. Int J Rail Transp 2013;1(1–2):57–73. http://dx.doi.org/10.1080/23248378.2013.788361.

[12] Indraratna B, Thakur P, Vinod J. Experimental and numerical study of railway ballast behavior under cyclic loading. Int J Geomech 2010;10(4):136–44. http://dx.doi.org/10.1061/(ASCE)GM.1943-5622.0000055, arXiv:http://dx.doi.org/10.1061/(ASCE)GM.1943-5622.0000055.

[13] Lu M, McDowell G. The importance of modelling ballast particle shape in the discrete element method. Granul Matter 2007;9(1–2):69–80. http://dx.doi.org/10.1007/s10035-006-0021-3.

[14] Ferellec J-F, McDowell GR. A method to model realistic particle shape and inertia in DEM. Granul Matter 2010;12(5):459–67. http://dx.doi.org/10.1007/s10035-010-0205-8.

[15] Huang H, Tutumluer E. Image-aided element shape generation method in discrete-element modeling for railroad ballast. J Mater Civ Eng 2014;26(3):527–35. http://dx.doi.org/10.1061/(ASCE)MT.1943-5533.0000839.

[16] Elias J. Simulation of railway ballast using crushable polyhedral particles. Powder Technol 2014;264:458–65. http://dx.doi.org/10.1016/j.powtec.2014.05.052.

[17] Harkness J, Zervos A, Le Pen L, Aingaran S, Powrie W. Discrete element simulation of railway ballast: modelling cell pressure effects in triaxial tests. Granul Matter 2016;18(3):1–13. http://dx.doi.org/10.1007/s10035-016-0660-y.

[18] Suhr B, Six K. Parametrisation of a DEM model for railway ballast under different load cases. Granul Matter 2017;19(4):64. http://dx.doi.org/10.1007/s10035-017-0740-7.

[19] Suhr B, Marschnig S, Six K. Comparison of two different types of railway ballast in compression and direct shear tests: experimental results and DEM model validation. Granul Matter 2018;20(4):70. http://dx.doi.org/10.1007/s10035-018-0843-9.

[20] Coetzee C. Review: Calibration of the discrete element method. Powder Technol 2017;310:104–42. http://dx.doi.org/10.1016/j.powtec.2017.01.015.

[21] Roessler T, Richter C, Katterfeld A, Will F. Development of a standard calibration procedure for the DEM parameters of cohesionless bulk materials – part I: Solving the problem of ambiguous parameter combinations. Powder Technol 2019;343:803–12. http://dx.doi.org/10.1016/j.powtec.2018.11.034.

[22] Suhr B, Six K. On the effect of stress dependent interparticle friction in direct shear tests. Powder Technol 2016;294:211–20. http://dx.doi.org/10.1016/j.powtec.2016.02.029.

[23] Suhr B, Six K. Friction phenomena and their impact on the shear behaviour of granular material. Comput Part Mech 2017;4:23–34. http://dx.doi.org/10.1007/s40571-016-0119-2.

[24] Kwan CCJ. Geogrid reinforcement of railway ballast (Ph.D. thesis), University of Nottingham; 2006.

[25] Quintanilla ID. Multi-scale study of the degradation of railway ballast (Ph.D. thesis), Universite Grenoble Alpes; 2018.

[26] Suhr B, Butcher TA, Lewis R, Six K. Cyclic friction tests of ballast stones interfaces under varying vertical load [dataset]. 2020, http://dx.doi.org/10.5281/zenodo.3893842, available at www.zenodo.org.

[27] Suhr B, Skipper WA, Lewis R, Six K. Shape analysis of railway ballast stones: curvature-based calculation of particle angularity. Sci Rep 2020;10. 6045. http://dx.doi.org/10.1038/s41598-020-62827-w.

[28] Archard JF. Contact and rubbing of flat surfaces. J Appl Phys 1953;24(8):981–8. http://dx.doi.org/10.1063/1.1721448.

[29] Krause H, Poll G. Wear of wheel-rail surfaces. Wear 1986;113(1):103–22. http://dx.doi.org/10.1016/0043-1648(86)90060-8.

[30] Lewis R, Braghin F, Ward A, Bruni S, Dwyer-Joyce R, Knani K, et al. Integrating dynamics and wear modelling to Predict railway wheel profile evolution. In: 6th Int. conf. contact mech. wear rail/wheel syst. C. CHARMEC. Gothenbg; 2003. URL https://pdfs.semanticscholar.org/510d/b1b239eceac9e90a45d34e949f39bd3b8d59.pdf.

[31] Six K, Meierhofer A, Müller G, Dietmaier P. Physical processes in wheel–rail contact and its implications on vehicle–track interaction. Veh Syst Dyn 2015;53(5):635–50. http://dx.doi.org/10.1080/00423114.2014.983675.

[32] Menezes P, Ingole S, Nosonovsky M, Kailas S, Lovell M, editors. Tribology for scientists and engineers. Springer; 2013.

[33] Chowdhury M, Khalil M, Nuruzzaman D, Rahaman M. The effect of sliding speed and normal load on friction and wear property of aluminum. Int J Mech Mechatronics Eng 2011;11(01):45–9.

[34] Quaglini V, Dubini P. Friction of polymers sliding on smooth surfaces. Adv Tribol 2011;178943. http://dx.doi.org/10.1155/2011/178943.

[35] El-Tayeb N, Gadelrab R. Friction and wear properties of e-glass fiber reinforced epoxy composites under different sliding contact conditions. Wear 1996;192(1):112–7. http://dx.doi.org/10.1016/0043-1648(95)06770-1.

[36] Berghold A. Wirkungsweise von unterschiedlichen Gleisschotterarten mit und ohne Schwellenbesohlung. ZEVrail 2016;1–2:140.

[37] Chen C, Indraratna B, McDowell G, Rujikiatkamjorn C. Discrete element modelling of lateral displacement of a granular assembly under cyclic loading. Comput Geotech 2015;69:474–84. http://dx.doi.org/10.1016/j.compgeo.2015.06.006.